Chemical Engineering Journal 155 (2009) 144–154

Contents lists available at ScienceDirect

Chemical Engineering Journal

journal homepage: www.elsevier.com/locate/cej

Modeling dye degradation kinetic using dark- and photo-Fenton type processes

Hrvoje Kusic, Natalija Koprivanac, Sanja Horvat, Saranda Bakija, Ana Loncaric Bozic*

Faculty of Chemical Engineering and Technology, University of Zagreb, Marulicev trg 19, Zagreb 10000, Croatia

ARTICLE INFO

Article history:
Received 22 April 2009
Received in revised form 2 July 2009
Accepted 13 July 2009

Keywords:
Fenton type processes
UV irradiation
Colored wastewater
Modeling
Sensitivity analysis

ABSTRACT

Dark- and photo-Fenton type processes, Fe^{2+}/H_2O_2, Fe^{3+}/H_2O_2, Fe^0/H_2O_2, $UV/Fe^{2+}/H_2O_2$, $UV/Fe^{3+}/H_2O_2$ and $UV/Fe^0/H_2O_2$, were applied for the treatment of model colored wastewater containing two reactive dyes, C.I. Reactive Blue 49 and C.I. Reactive Blue 137, and degradation kinetics were compared. Dye degradation was monitored by the means of UV/VIS, adsorbable organic halides (AOX) and total organic carbon (TOC) analysis, thus determining decolorization and dechlorination of triazine structure, as well as mineralization of model colored wastewater. Both dark- and photo-Fenton type processes were proven to be very efficient for color removal; ≥98% was achieved in all cases. Significant improvements in the mineralization of studied dyes were achieved by the assistance of UV light, as it was expected. It was demonstrated that the degradation kinetic of applied dyes depended on the presence of UV light, as well as type of iron catalyst and dye structure. On bases of the obtained experimental results, the mathematical models were developed describing dye degradation kinetics in all studied systems. Since UV light was used in order to enhance the efficiency of dark-Fenton type processes, mathematical model describing dye degradation by UV photolysis providing the values of quantum yields for each of the dye was developed and incorporated in model for photo-Fenton type processes. A sensitivity analysis for the evaluation of importance of each reaction used in mathematical models was also performed.

1. Introduction

The manufacturing and application of synthetic dyes involve the production of large amounts of colored wastewater which may cause serious threat to the human health and the environment. Thus, efficient treatment of colored wastewater prior to discharge into the natural water bodies is demanded. Conventional treatment operations for colored wastewater include biological and physical methods and their combinations such as aerobic and anaerobic digestion, carbon adsorption and coagulation/flocculation, which are often proven to be insufficiently effective. Their shortcomings can be overcome by the application of an appropriate advanced oxidation process (AOP) [1–6].

It was shown that dark-Fenton type processes ensure effective decolorization of model wastewater containing reactive dyes, but in most cases, significant mineralization degree could not be reached [7]. Although applied systems offer a cost effective source of $HO^{\bullet}$, their efficiency is limited due to the formation of stable Fe^{3+}-complexes [8,9]. By the assistance of UV irradiation, formed complexes are degraded, thus allowing Fe^{3+} ions to participate in the Fenton catalytic cycle, Eq. (1) [10,11]:

$$Fe^{3+}\text{-complex} + h\nu \rightarrow Fe^{2+} + \text{organicproducts} \quad (1)$$

Generally, organic molecules could be degraded by UV irradiation [12], but the efficiency of direct photolysis of dye was shown to be rather poor and dependent on dye concentration, as well as on its reactivity and photosensitivity [13,14]. Moreover, many of the commercially used dyes are designed to be light resistant. In photo-Fenton type process, besides destruction of stable Fe^{3+}-complexes, UV irradiation enables additional OH radical generation through the photolysis of H_2O_2 and the reduction of Fe^{3+} ions, Eqs. (2) and (3), respectively [9,12]:

$$H_2O_2 + h\nu \rightarrow 2OH^{\bullet} \quad (2)$$

$$Fe^{3+} + H_2O + h\nu \rightarrow Fe^{2+} + HO^{\bullet} + H^{+} \quad (3)$$

The goal of the study was to investigate and compare the degradation efficiency and the kinetic of dark-, Fe^{2+}/H_2O_2, Fe^{3+}/H_2O_2 and Fe^0/H_2O_2, and photo-, $UV/Fe^{2+}/H_2O_2$, $UV/Fe^{3+}/H_2O_2$ and $UV/Fe^0/H_2O_2$, Fenton type processes for the treatment of model colored wastewater. Typical representatives of monochlorotriazine reactive dyes, with anthraquinone and azo chromophore, C.I. Reactive Blue 49 and C.I. Reactive Blue 137 respectively, were used as model pollutants. Apart from the experimental work, a detailed mathematic modeling of dye degradation was performed in order

* Corresponding author. Tel.: +385 1 4597 123; fax: +385 1 4597 143.
E-mail address: abozic@fkit.hr (A.L. Bozic).

1385-8947/$ – see front matter © 2009 Elsevier B.V. All rights reserved.
doi:10.1016/j.cej.2009.07.029

to describe applied dark- and photo-Fenton type processes in laboratory batch scale. Such study provided important information on system behavior dependent on structure of model pollutant, type of iron catalyst and the presence of UV light, thus influencing the overall process efficiency. Sensitivity analysis was performed to evaluate importance and contribution of each reaction used to describe dye degradation mechanism proposed by developed mathematical models for each studied system. As an integral part of the study the kinetic modeling of UV photolysis was also performed. The purpose was to (i) provide values of quantum yield for each of the studied dye as an important, structurally related photochemical parameter and to (ii) incorporate developed model in mathematical models describing behavior of photo-Fenton type processes.

2. Experimental

Two reactive dyes C.I. Reactive Blue 49 (RB49) and C.I. Reactive Blue 137 (RB137) were used as model wastewater pollutants in concentration of 20 mg L^{-1}. In this work, experiments were conducted at previously determined optimal operating conditions for each dark-Fenton type process as well as studied colored pollutant [7,15]. All experiments were performed in the batch photoreactor described in details elsewhere [11,16,17]. UV lamp (typical intensity on 2 cm ≈ 4.4 mW cm^{-2}) was located in the middle of the reactor in a quartz tube. The value of incident photon flux at 254 nm, $I_0 = 3.68 \times 10^{-6}$ Einstein s^{-1}, was calculated on the basis of hydrogen peroxide actinometry measurements [18]. In dark-Fenton type processes the UV lamp was off. The total volume of the treated solution was 0.5 L, while the mixing was provided by magnetic stirring bar. Temperature was maintained at 25 ± 0.2 °C by circulating the water through the jacket around the photoreactor. The duration of each experiment was 120 min; samples were taken periodically from the reactor (0, 2, 5, 15, 30, 45, 60, 75, 90, 105, 120 min) and thereafter immediately analyzed. All experiments were repeated at least three times and averages were reported, while reproducibility of the experiments was within 5%.

A PerkinElmer Lambda EZ 201 UV/VIS spectrophotometer was used for the monitoring of UV/VIS spectral changes of both dyes in the region 200–800 nm, as well as to determine the concentrations of iron ions in the bulk during the treatment by applied processes. Ferrous ions were identified by the reaction of Fe^{2+} with 1,10-phenanthroline giving orange–red complex (λ_{max} = 510 nm), while ferric ions were determined by the reaction of Fe^{3+} with thiocyanate forming under acidic conditions a red-colored complex (λ_{max} = 480 nm) [19]. Dechlorination of a triazine part of RB49 and RB137 was evaluated by measuring absorbable organic halides

Table 1
The reactions, rate constants and quantum yields used for the kinetic modeling.

#	Reaction	Reference	k (M^{-1} s^{-1})	
			Lit.	Used
1	$Fe^{2+} + H_2O_2 \rightarrow Fe^{3+} + OH^\bullet$	[11,20–25]	63–76	76
2	$Fe^{3+} + H_2O_2 \rightarrow Fe^{2+} + H^+ + HO_2^\bullet$	[11,20–25]	0.01–0.02	0.02
3	$Fe^{2+} + OH^\bullet \rightarrow Fe^{3+} + OH^-$	[11,20–24]	$3.0–4.3 \times 10^8$	3.2×10^8
4	$Fe^{3+} + HO_2^\bullet \rightarrow Fe^{2+} + O_2 + H^+$	[11,20–24]	$0.1–3.1 \times 10^5$	3.1×10^5
5	$Fe^{2+} + HO_2^\bullet \rightarrow Fe^{3+} + HO_2^-$	[11,20–24]	1.2×10^6	1.2×10^6
6	$Fe^{3+} + O_2^{\bullet-} \rightarrow Fe^{2+} + O_2$	[11,20–24]	$0.5–1.5 \times 10^8$	5.0×10^7
7	$Fe^{2+} + O_2^{\bullet-} \rightarrow Fe^{3+} + H_2O_2$	[11,20–24]	1.0×10^7	1.0×10^7
8	$OH^\bullet + H_2O_2 \rightarrow HO_2^\bullet + H_2O$	[11,20–24]	$1.2–4.5 \times 10^7$	4.5×10^7
9	$2OH^\bullet \rightarrow H_2O_2$	[11,21–24]	$4.2–5.3 \times 10^9$	5.3×10^9
10	$HO_2^\bullet + OH^\bullet \rightarrow H_2O + O_2$	[11,21–24]	6.6×10^{11}	6.6×10^{11}
11	$2HO_2^\bullet \rightarrow H_2O_2 + O_2$	[11,20–24]	8.3×10^5	8.3×10^5
12	$O_2^{\bullet-} + HO_2^\bullet \rightarrow HO_2^- + O_2$	[11,20–24]	9.7×10^7	9.7×10^7
13	$O_2^{\bullet-} + HO^\bullet \rightarrow HO^- + O_2$	[16,21–23]	1.0×10^{10}	1×10^{10}
14	$HO_2^\bullet \rightarrow O_2^{\bullet-} + 2H^+$	[11,20–24]	$1.58–7.9 \times 10^5$ s^{-1}	1.58×10^5 s^{-1}
15	$O_2^{\bullet-} + 2H^+ \rightarrow HO_2^\bullet$	[11,20–24]	1.0×10^{10}	1.0×10^{10}
16	$OH^\bullet + H_2O_2 \rightarrow O_2^{\bullet-} + H_2O$	[16,22,23]	2.7×10^7	2.7×10^7
17	$Fe^0 + H^+ \rightarrow Fe_{surface}^{2+} + H_2$	[11,25,26]		4.17×10^{-4}
18	$Fe_{surface}^{2+} + H_2O_2 \rightarrow Fe_{surface}^{3+} + OH^\bullet$			76
19	$Fe_{surface}^{3+} + H_2O_2 \rightarrow Fe_{surface}^{2+} + H^+ + HO_2^\bullet$			0.02
20	$Fe_{surface}^{2+} + OH^\bullet \rightarrow Fe_{surface}^{3+} + OH^-$			3.2×10^8
21	$Fe_{surface}^{3+} + HO_2^\bullet \rightarrow Fe_{surface}^{2+} + O_2 + H^+$			3.1×10^5
22	$Fe_{surface}^{2+} + HO_2^\bullet \rightarrow Fe_{surface}^{3+} + HO_2^-$			1.2×10^6
23	$Fe_{surface}^{3+} + O_2^{\bullet-} \rightarrow Fe_{surface}^{2+} + O_2$			5.0×10^7
24	$Fe_{surface}^{2+} + O_2^{\bullet-} \rightarrow Fe_{surface}^{3+} + H_2O_2$			1.0×10^7
25	$Fe_{surface}^{2+} + H^+ \rightarrow Fe^{2+} + H_2$	[11,26]		7.83×10^{-3}
26	$H_2O_2 + h\nu \rightarrow 2OH^\bullet$	[11,12,20,27]	Φ = 0.5 mol Einstein^{-1}	Φ = 0.5 mol Einstein^{-1}
27	$OH^\bullet + HO_2^- \rightarrow HO_2^\bullet + OH^-$	[24,27]	7.5×10^9	7.5×10^9
28	$HO_2^\bullet + H_2O_2 \rightarrow H_2O + HO^\bullet + O_2$	[27]	3.0	3.0
29	$O_2^{\bullet-} + H_2O_2 \rightarrow OH^- + HO^\bullet + O_2$	[27]	0.13	0.13
30	$Fe^{3+} + H_2O + h\nu \rightarrow Fe^{2+} + OH^\bullet + H^+$	[9–11,20,28]		3.33×10^{-6}
31	$PDM + h\nu \Leftrightarrow PDM^* \rightarrow CLP$			Φ_{RB49} = 7.2 mmol Einstein^{-1} Φ_{RB137} = 4.2 mmol Einstein^{-1}
32	$OC + h\nu \Leftrightarrow OC^* \rightarrow IP$			Φ_{RB49} = 3.6 mmol Einstein^{-1} Φ_{RB137} = 5.3 mmol Einstein^{-1}
33	$PDM + OH^\bullet \rightarrow CBP$	[29] [17]	1.33×10^9 for RB49 3.32×10^9 for RB137	1.33×10^9 for RB49 3.32×10^9 for RB137
34	$OC + OH^\bullet \rightarrow IP$	[17]	2.68×10^8	2.68×10^8
35	$OC + OH^\bullet \rightarrow OP$			$0.90–5.17 \times 10^{8*}$
36	$Fe^{3+} + OP \rightarrow Fe^{3+}$-complexes	[11,21]	1.0	1.0
37	$Fe_{surface}^{3+} + OP \rightarrow Fe_{surface}^{3+}$-complexes			1.0
38	Fe^{3+}-complexes $+ h\nu \rightarrow Fe^{3+} + OC$	[11]	1×10^{-3} s^{-1}	1×10^{-3} s^{-1}
39	$Fe_{surface}^{3+}$-complexes $+ h\nu \rightarrow Fe^{3+}{}_{surface} + OC$			1×10^{-3} s^{-1}

PDM: Parent dye molecule, CLP: colorless by-products, OC: organic content, IP: inorganic products, OP: organic products (capable to form stable complexes with Fe^{3+} ions).
* Structure of organic pollutant and type of iron catalyst dependent.

Table 2
Values of calculated standard deviation (SD) for each of model–experiment data pairs presented in Figs. 3–6 and 8–11.

Process	SD					
	RB49				RB137	
	Color removal	TOC removal	H_2O_2 consumption	Fe ions leaching	Color removal	TOC removal
UV	0.0212	0.0024	–	–	0.0026	0.0083
Fe^{2+}/H_2O_2	0.0149	0.0128	0.0067	–	0.0065	0.0123
$UV/Fe^{2+}/H_2O_2$	0.0120	0.0097	–	–	0.0012	0.0115
Fe^{3+}/H_2O_2	0.0255	0.0089	0.0055	–	0.0024	0.0080
$UV/Fe^{3+}/H_2O_2$	0.0096	0.0049	–	–	0.0036	0.0103
Fe^{0}/H_2O_2	0.0157	0.0115	0.0176	0.0063	0.0193	0.0088
$UV/Fe^{0}/H_2O_2$	0.0288	0.0086	–	–	0.0059	0.0143

content (AOX), performed by Organic Halide Analyzer, DX-2000, Dohrmann. Mineralization extents were determined on the basis of total organic carbon content measurements (TOC), using Total Organic Carbon Analyzer; TOC-V_{CPN}, Shimadzu. Handylab pH/LF portable pH-meter, Schott Instruments GmbH, Mainz, Germany, was used for adjusting initial pH at desired value. The consumption of hydrogen peroxide during the treatment by applied processes was monitored using modified iodometric titration method [19].

3. Model formulation

The mathematical models for Fenton type processes, including 20 chemical species (ions, atoms and molecules) and 39 chemical reactions, were developed using chemical reactions and rate constants mostly from literature, including our previous studies (Table 1) [9–11,20–29]. The developed models describe radical chain reactions which occur in the bulk and at the surface of iron powder (when used as a source of iron catalyst) during degradation of model colored solutions by applied Fenton type processes. Number of chemical species and chemical reactions included in each model for specific Fenton type process varied depending on whether process was performed in the dark or in the presence of UV light and which type of iron catalyst was used. The general mass balance for a well-mixed, constant volume and constant temperature batch reactor is given by:

$$\frac{dc_i}{dt} = -r_i \quad (1)$$

where c_i is concentration of specie i in the bulk and r_i is the bulk phase rate of the same specie [30]. Dye degradation was simulated by *Mathematica 5.0* (Wolfram Research, Champaigne, IL) using GEAR method which finds the numerical solution to the set of ordinary differential equations. Values of the rate constants of reactions, #17, #25, #35, #38, and #39, and quantum yields, #31 and #32 (Table 1), were determined by trial and error method fitting the values into the model. Models were developed in following manner. Model describing Fenton mechanism in homogeneous system, i.e. using either Fe^{2+} or Fe^{3+} salts, was considered as the basic one and the values of the rate constants of reaction #35 (Table 1) were determined depending on dye structure and the type of iron salt, using above described trial and error method. According to the literature [26,31], several hypotheses were used in development of the model describing the behavior of dark heterogeneous process using iron powder as a source of iron catalyst. It was assumed that Fenton reactions occur simultaneously at the surface and in the bulk, while the portion occurring in the bulk depends on experimental conditions influencing the rate of iron dissolution. The value of rate constant for reaction #25 is determined on the basis of experimentally obtained data for iron bulk profile. The same rate constants for the well-known reactions describing bulk reactions of Fenton catalytic cycle were used for the surface reactions. The limiting factor of Fenton surface reactions is generation of active $Fe_{surface}^{2+}$ sites. The rate constant of reaction #17 was determined on the basis of experimentally obtained H_2O_2 consumption profile and mineralization of organic content. Before developing the models which describe the behavior of photo-Fenton type processes, the model predicting the photolysis of colored model wastewaters was developed. This model predicts the values of quantum yields of used dyes and overall organic content. The model was afterwards incorporated in both final models, homogeneous and heterogeneous, describing the degradation of colored model solutions by photo-Fenton type processes. In these final models, the values of rate constants for two reactions, #38 in homogeneous model and #39 in heterogeneous model (Table 1.), were determined. Fitting of the models was evaluated on the basis of calculated values of standard deviation (SD) for each model–experiment data pair (Table 2).

In order to determine the sensitivity of the model output to input reaction rate constants and the importance of specific reactions, a parametric sensitivity analysis, described in details in the literature [32,33], was used. In this study the peak values of normalized sensitivity coefficient are reported, and in the all cases these peak values occurred at time 120 min, where the observed parameter *inorganic products*, i.e. mineralized part of model colored wastewater (IP, expressed as a removed TOC value) is at the highest concentration. Only reactions with sensitivity coefficients within 2–3 orders of magnitude of the most sensitive reaction are reported.

4. Results and discussion

4.1. Direct UV photolysis

Before focusing on the investigation of photo-Fenton type processes for the degradation of RB49 and RB137, a set of experiments was performed, where both studied dyes were degraded by UV irradiation alone. Figs. 1 and 2 show the absorption spectral changes during the direct photolysis of RB49 and RB137, respectively.

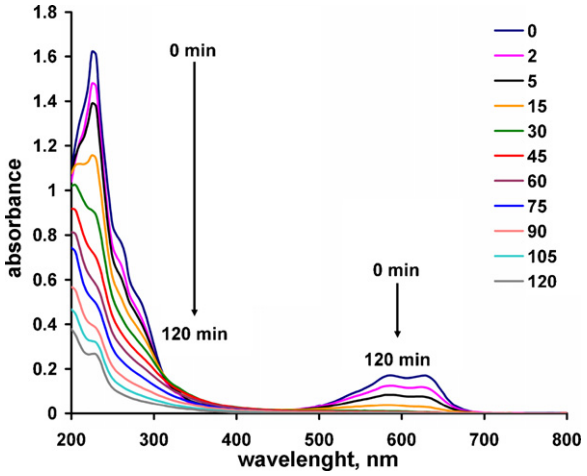

Fig. 1. Changes in UV/VIS absorbance spectra during direct photolysis of RB49.

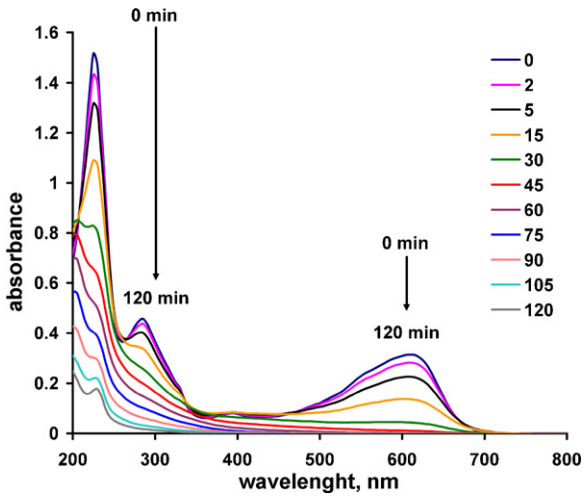

Fig. 2. Changes in UV/VIS absorbance spectra during direct photolysis of RB137.

Absorption spectrum of RB49, reactive dye with anthraquinone chromophore, is characterized by one pronounced band in UV region with maxima at 230 nm, and another in VIS region, at 590 and 630 nm (Fig. 1). The absorbance peak at 230 nm can be mainly contributed to the triazine ring in dye structure [34], while expected absorbance of aromatic structures in UV region is not pronounced. The spectral bands at 590 and 630 nm correspond to the chromophore of RB49 dye, and 590 nm was chosen as λ_{max} for monitoring decolorization of RB49. Absorption spectra of RB137, reactive dye with azo chromophores, is characterized by two pronounced bands in UV region, with absorbance peaks at 230 and 280 nm, and one in VIS region with absorbance peak at 610 nm (Fig. 2). The absorbance peaks in UV region, at 230 and 280 nm, can be contributed to the triazine and benzene rings, respectively [34]. The spectral band at 610 nm corresponds to the chromophore of RB137, and it was chosen as λ_{max} for monitoring decolorization of RB137 in further study. From Figs. 1 and 2 it can be seen that spectral bands in visible region disappear much faster than those in UV region. Moreover, in less than 60 min of treatment, both model solutions were completely decolorized and correspondingly no spectral bands in VIS region were recorded. On the other hand, spectral bands in UV region were still present, indicating the incomplete mineralization of organics in model wastewaters.

In Figs. 3 and 4 decolorization and mineralization kinetics of RB49 and RB137 by direct photolysis are compared with the

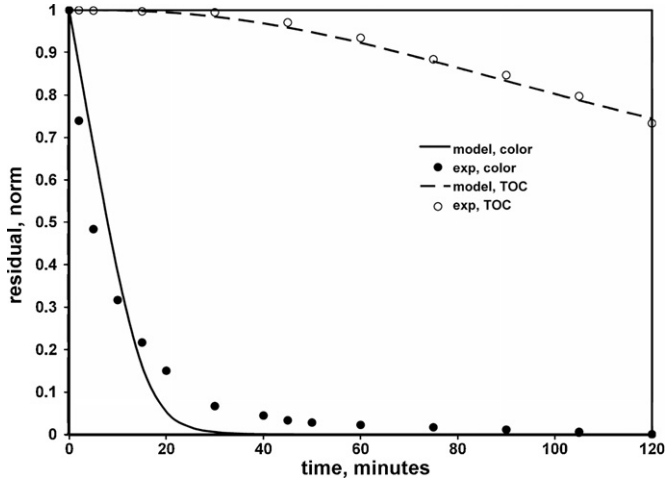

Fig. 3. Degradation kinetic of RB49 by direct photolysis, the comparison of model and experimental data.

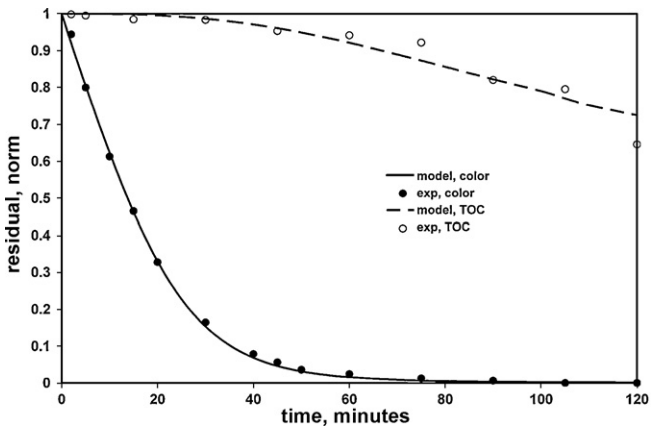

Fig. 4. Degradation kinetic of RB137 by direct photolysis, the comparison of model and experimental data.

results predicted by developed mathematical model. As it was pointed out earlier, both model colored solutions were completely and rather fast decolorized by direct photolysis. Slight difference in decolorization rates at the beginning of UV photolysis could be contributed to the structural properties of the dyes and related physical properties of the model solutions, expressed by the means of quantum yield and molar absorption coefficient. Therefore, the decolorization of both dyes by direct UV photolysis was monitored and the quantum yields of RB49 and RB137 were calculated on the basis of mathematical modeling. The quantum yields of RB49, $\Phi_{RB49} = 7.2 \times 10^{-3}$ mol Einstein^{-1}, and RB137, $\Phi_{RB137} = 4.2 \times 10^{-3}$ mol Einstein^{-1}, were determined by trial and error method inserting the values into the model with simultaneous comparison of predicted and experimentally obtained data for RB49 and RB137 decolorization, respectively. In that purpose a modified version of a semiempirical "LL model" based on the Lambert's law was used, Eq. (5) [12]:

$$r_{UV} = -\frac{dc_i}{dt} = \Phi_i \times F_i \times I_0 \times \left[1 - \exp(-2.303 \times L \times \sum \varepsilon_j \times c_j)\right] \quad (5)$$

being $F_i = \varepsilon_i \times c_i / \sum \varepsilon_j \times c_j$Other constants presented in above Eq. (5), Φ_i, ε_i, I_0 and L, stand for the physical properties of specie i, its quantum yield and the extinction coefficient, as well as the incident photon flux by reactor volume unit and the effective optical path in the reactor, respectively. Taking into the consideration only the beginning of the photolysis process, it can be assumed that almost all radiation was adsorbed by the parent compound i. In the latter case, it follows that $\varepsilon_i c_i \approx \varepsilon_j c_j$ and $F_i \approx 1$. Consequently, Eq. (5) could be modified as [35]:

$$r_{UV} = -\frac{dc_i}{dt} = \Phi_i \times I_0 \times [1 - \exp(-2.303 \times L \times \varepsilon_i \times c_i)] \quad (6)$$

Knowing the values of I_0 and L (in our case 3 cm), the quantum yield of the specie i could be calculated, as it was done in our case. The values of extinction coefficients of RB49, $\varepsilon_{0,RB49} = 34{,}122\ M^{-1}\ cm^{-1}$, and RB137, $\varepsilon_{0,RB137} = 18{,}124\ M^{-1}\ cm^{-1}$, were calculated from Eq. (7) by measuring absorbance of RB49 or RB137 solution at 254 nm. Absorbance A, can be expressed as:

$$A = \varepsilon \times l \quad (7)$$

where ε is the molar absorption coefficient with dimensions 1/(concentration × length), and l is the cell path length [36]. The applied model (Eq. (6)) showed good correlation with the experimentally obtained results for decolorization, especially in the case of RB137 dye ($SD_{RB49,color} = 0.0212$ and $SD_{RB137,color} = 0.0026$). However, from the experimental results obtained for both model colored wastew-

aters (Figs. 3 and 4), it can be seen that at the beginning of the photolysis, mineralization proceeds rather slowly and mineralization extent is almost negligible until certain level of decolorization is achieved. Such behavior during degradation of colored wastewater is in accordance with the literature [37]. Therefore, the model (6) used for decolorization kinetic required several modifications in order to be suitable for prediction of the mineralization of model colored solutions. Consequently, the model (6) was modified in the following manner:

$$-\frac{dc_{TOC}}{dt} = z_t \times \Phi_{TOC} \times I_0 \times [1 - \exp(-2.303 \times L \times \varepsilon_{TOC,t} \times c_{TOC,t})] \quad (8)$$

where z_t is dimensionless time depended variable given by:

$$-\frac{dz}{dt} = \frac{|(c_{dye,t} \times M_{dye})/\gamma_{dye,0} - (c_{TOC,t} \times M_{TOC})/\gamma_{TOC,0}|}{\varepsilon_{color,t}/\varepsilon_{TOC,t}} \quad (9)$$

with the physical meaning which describes previously mentioned dependence of the level of color removal and the rate of mineralization. Additionally, $\varepsilon_{color,t}$ and $\varepsilon_{TOC,t}$ represent the time depended extinction coefficients of parent pollutant, dye, and overall organic content, calculated on the basis of Eq. (7). After above shown modifications, model gave a very good prediction of mineralization results in the cases of both colored pollutants (Figs. 3 and 4). The quantum yields of organic contents of both model solutions, $\Phi_{TOC,RB49} = 3.6 \times 10^{-3}$ mol Einstein^{-1}, and RB137, $\Phi_{TOC,RB137} = 5.3 \times 10^{-3}$ mol Einstein^{-1}, were determined by model (8) using earlier mentioned trial and error method ($SD_{TOC,RB49} = 0.0024$ and $SD_{TOC,RB137} = 0.0083$, Table 2). The plausible explanation for different values of calculated quantum yield for organic content in the case of RB49 and RB137 could be that due to the different structure partially mineralized solutions could contain different organic by-products. At the end, some general conclusions on the basis of experimental results presented in Figs. 1–4 can be made. Decolorization rates are relatively high in comparison to mineralization rates (Figs. 3 and 4). Also, only partial mineralization of RB49 and RB137 solution were obtained, 26.7% and 35.4% of TOC removal, respectively. This is in accordance with the results presented in Figs. 1 and 2, where spectral bands corresponding to aromatic structures were still present in UV region even after 120 min of treatment. Although it could be assumed that triazine structures were degraded with the lowest rate by direct photolysis due to the remaining spectral bands with maxima at 230 nm (Figs. 1 and 2), the final values of AOX in comparison to TOC removals of RB49 and RB137 were rather high, 77.7% and 83.1% respectively. This suggests that structures absorbing in UV region, other than triazine, contribute to the remained spectral bands. According to some authors [34], the degradation of triazine structures is favored by UV photolysis. On the other hand, Feng et al. [38] suggest that triazine structures are much more resistant to the degradation by OH radicals than other aromatic structures in dye molecule. Therefore, it can be concluded that remaining bands in the UV region (Figs. 1 and 2) correspond to the either aromatic or aliphatic intermediates of partial degradation of parent dye molecules due to the predominance of UV photolysis mechanism over OH radical mechanism in the UV process.

4.2. Fenton, Fe^{2+}/H_2O_2, and photo-Fenton, $UV/Fe^{2+}/H_2O_2$, processes

The next step of the study was the development of mathematical models for predicting the degradation of model colored wastewaters by Fenton type processes, both dark and photo. In that purpose dark- and photo-Fenton processes using Fe^{2+} salt as a source of iron catalyst were applied for degradation of model colored wastewaters. The influence of operating process parameters for the

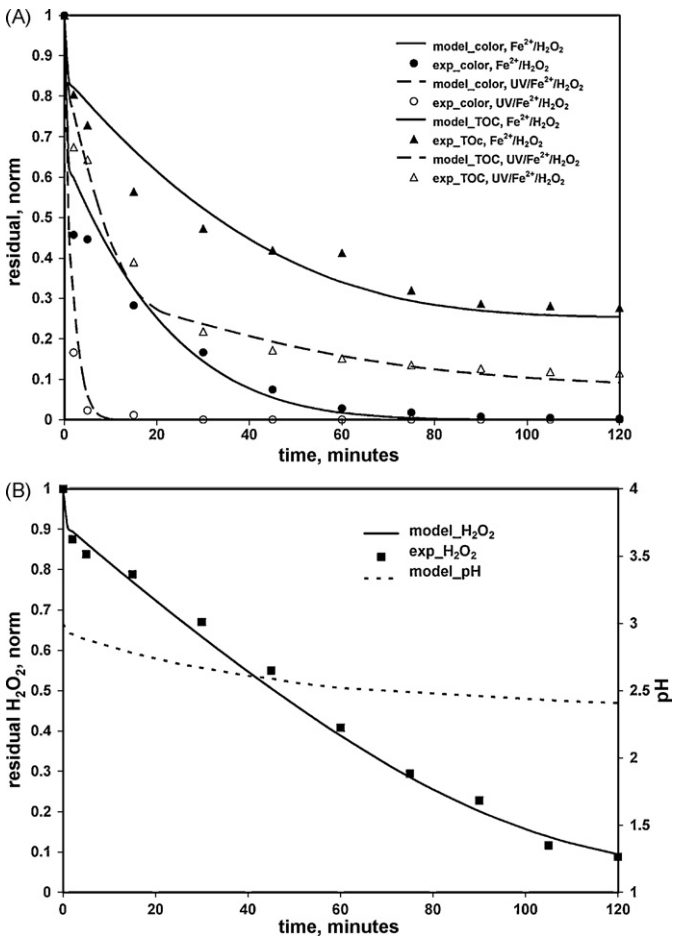

Fig. 5. (A) Degradation kinetic of RB49 by Fe^{2+}/H_2O_2 and $UV/Fe^{2+}/H_2O_2$ processes, the comparison of model and experimental data, (B) H_2O_2 consumption during degradation of RB49 by Fe^{2+}/H_2O_2, the comparison of model and experimental data.

degradation of both studied dyes of Fenton process, Fe^{2+}/H_2O_2 was studied previously [7], and the conditions yielding with the highest dye degradation efficiency were established. This work was focused on the comparison of degradation kinetic of RB49 and RB137 by dark- and photo-Fenton processes, and development of the appropriate models to predict one. In Fig. 5(A) experimentally obtained kinetic of decolorization and mineralization of RB49 by dark- and photo-Fenton processes ($[Fe^{2+}] = 0.5$ mM, $Fe^{2+}/H_2O_2 = 1{:}20$, pH 3) is compared with the data predicted by developed models. The much faster decolorization of RB49 by photo-Fenton than by dark-Fenton process can be primarily contributed to the additional production of OH radicals by the photolysis of H_2O_2 (Table 1, #26), and also to the direct photolysis of dye molecule (Table 1, #31). However, after 120 min of the treatment by both Fe^{2+}/H_2O_2 and $UV/Fe^{2+}/H_2O_2$ processes, differences between final decolorization extents are almost negligible. On the other hand, the positive effect of UV irradiation can be observed from the mineralization curves (Fig. 5(A)). Mineralization of RB49 solution by photo-Fenton is rather faster than by dark-Fenton process. Moreover, $UV/Fe^{2+}/H_2O_2$ yielded with the higher final mineralization extent. After 120 min of treatment, the TOC value of RB49 solution was decreased for 72.4% by dark-Fenton process, while 88.5% mineralized by the same process in the light. However, similar trends in mineralization curves for both dark- and photo-Fenton processes can be observed. After relatively fast initial mineralization, the curves showed significant leveling off. The pronounced slowing in the mineralization rate after 15 min of treatment by dark-Fenton process can be contributed to the pre-

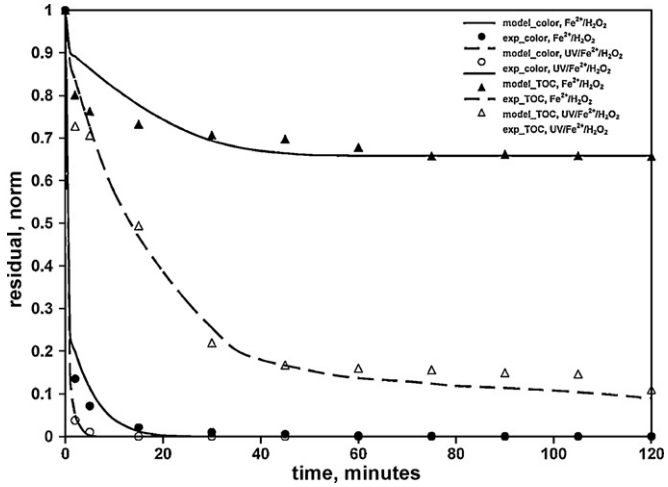

Fig. 6. Degradation kinetic of RB137 by Fe^{2+}/H_2O_2 and UV/Fe^{2+}/H_2O_2 processes, the comparison of model and experimental data.

cluding of Fe^{3+} ions from the catalytic cycle due to the formation of stable Fe^{3+}-complexes between iron ions and carboxylic acids as aliphatic by-products of dye degradation [8]. These complexes can be degraded under UV irradiation resulting with higher mineralization extent, obtained by photo-Fenton process (Fig. 5(A)). Also, aliphatic compounds, such as oxalic, acetic and maleic acids, which are known to be the products of organic dye degradation [39,40], are resistant to oxidation by Fenton reactions [8], thus contributing to the remained organic content after dark-Fenton process. These organic acids can be degraded under UV light, but due to the low molar absorption at 254 nm, reaction rates are correspondingly low [34,41]. This can be a plausible explanation for the observed leveling off in mineralization curve of photo-Fenton process. However, trend of the curve in the last 30 min of the process indicates that mineralization would proceed with the extended treatment time. Taking into account the well-known mechanism regarding the Fenton catalytic cycle and side reactions occurring in the bulk [8–11,20–24] as well as observed behavior of the studied system during degradation by dark- and photo-Fenton processes, the mathematical models were developed. The degradation of model colored wastewater by dark-Fenton process was described using reactions #1–16, #34–36 (Table 1), while the model for photo-Fenton process was develop by upgrading model for dark process by additional specific reactions #26–30 and #37 (Table 1), and incorporating in it the earlier developed model for UV process (Eqs. (6) and (8)). The results of the model–experiment comparison are given in Fig. 5(A) and (B) comparing the model and experimental data for dye degradation (decolorization and mineralization) by both processes and the consumption of H_2O_2 during dark-Fenton process, respectively. It can be seen that models describe system behavior with a very good accuracy (Table 2). The value of rate constant for the reaction #35 (Table 2) presenting a formation of complex-suitable (CS) compounds by the degradation of initial organic content (OC) with OH radicals, was calculated by trial and error method. That reaction describes the earlier mentioned typical leveling off in rate of mineralization occurring in dark-Fenton process (Fig. 5(A)). The value of the rate constant of that reaction depends on the type of the dye, i.e. in the manner in which the organic pollutant when degraded is capable to form CS compounds.

The same models were tested in the case of another studied colored pollutant, RB137, and results of degradation by Fe^{2+}/H_2O_2 and UV/Fe^{2+}/H_2O_2 processes ([Fe^{2+}] = 0.5 mM, Fe^{2+}/H_2O_2 = 1:30, pH 3) are compared in Fig. 6. It can be seen that models showed a good predictability for the studied systems, providing a satisfactory fitting of model to experimental results (SD values are listed in Table 2). Several observations can be made according to the experimentally obtained results. Decolorization proceeded with almost the similar rate in both cases and yielded with more than 95% after 2 min of treatment in both cases. The difference in final decolorization extent, 98% in the dark and 100% in the light, is almost negligible. One of the major observations is based on the comparison of data presented in Figs. 5 and 6, leading to the conclusion that dye structure plays significant role in degradation mechanism. Model solution of RB137 with azo chromophore was easily decolorized by both dark- and photo-Fenton processes. On the other hand, RB49 dye with anthraquinone chromophore was shown to be more stable in the dark, and the positive effect of UV assistance to the decolorization rate is more pronounced. That part was described in the model with different rate constants for decolorization, where higher one was given to RB137, while positive effect of UV irradiation providing faster degradation of RB49 in photo-Fenton process can be contributed to the higher quantum yield of RB49, indicating less resistance of that dye to UV degradation (already shown in Fig. 3). Also, from Fig. 6 it can be seen that after 2 min of Fe^{2+}/H_2O_2 process, mineralization of RB137 was significantly slowed down, almost inhibited. Assuming that the formation of iron complexes with dye degradation products is the main reason for such behavior, it can be concluded that after 2 min such complexes are formed and only a very small portion of Fe^{3+} still participated in Fenton catalytic cycle. In Fenton type processes besides OH radicals, the role of organic radicals in overall degradation throughout radical chain mechanism should not be neglected [20,42]. Formation of degradation products, their nature and characteristics, is strongly dependent on the structure of parent dye molecule [42–45]. Obtained results for the dark-Fenton processes indicate that in the case of azo dye (Fig. 6), the formation of iron-complexing species leads to the inhibition of Fenton reactions. On the other hand, in the case of anthraquinone dye (Fig. 5), the formation of organic radicals capable to participate in chain reactions prevails, thus contributing to the overall mineralization extent. Lachheb et al. [44] demonstrated that different molecular structures of the dyes influence on their reactivity with OH radicals which constitute the main oxidizing agents generated in UV-irradiated aqueous suspensions of titania, similarly like in dark- and photo-Fenton processes presented in this study. Therefore, the value of rate constant of reaction #35 (Table 2) for the system containing RB137 was much higher than in the case of RB49.

The importance of this reaction and its influence on the prediction of studied system is supported by the performed sensitivity analysis. Results of the sensitivity analysis, presenting the peak values of normalized sensitivity coefficients for the concentration of inorganic products of dye solution (IP) with respect to the rate constant of chemical reactions used in kinetic modeling are given in Fig. 7(A) and (B) for dark- and photo-Fenton processes, respectively. Positive results of the normalized sensitivity coefficient for IP indicate that if the particular reaction rate constant was increased, a lower IP concentration would occur, showing that the rate of mineralization (#34) would be lower. On the other hand, negative values of the IP sensitivity coefficients indicate that mineralization yield is increasing with an increase in the reaction rate. What is important, the sensitivity analysis shows the magnitude of the increase or decrease in IP concentration, and therefore describes the significance of the specific reaction. The value for the normalized sensitivity coefficients gives the order of magnitude of the change in concentration if the given reaction parameter changes by an order of magnitude. Hence, if the value of sensitivity coefficient for IP is 1, that would indicate that if reaction rate were increased by 1 order of magnitude, the value of IP concentration would be 1 order of magnitude higher than the original reaction rate [24,32,33]. In this study, sensitivity analysis performed for the model describing

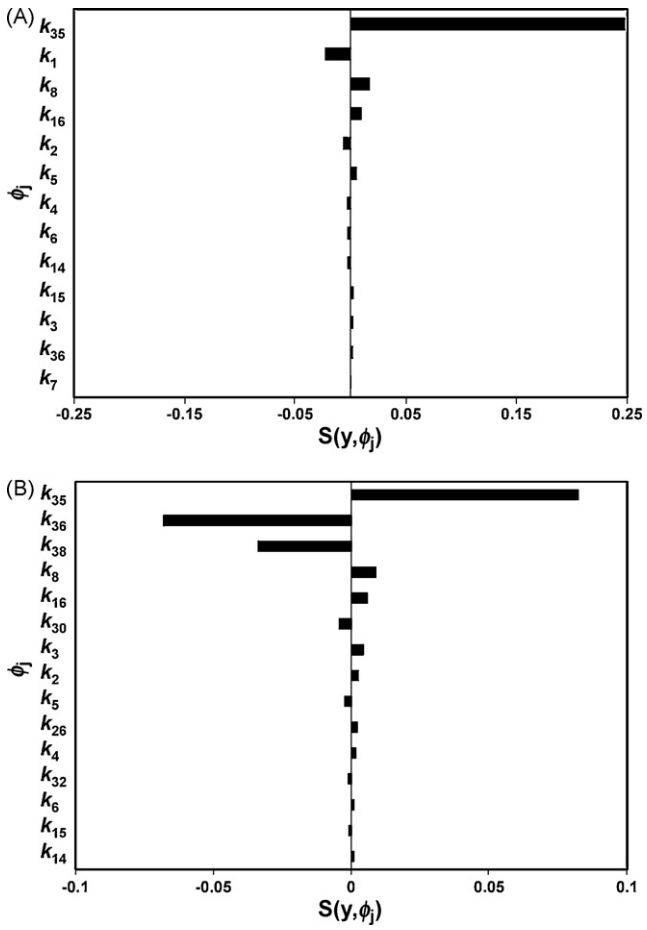

Fig. 7. The peak values of the normalized sensitivity coefficients for the concentration of inorganic products (IP) with respect to reaction rate constant for the chemical reactions used in kinetic modeling; (A) dark-Fenton and (B) photo-Fenton processes.

dark-Fenton process for degradation of model colored wastewater showed that the most important reaction in the investigated system, besides reaction between OC and OH radicals giving IP (Table 1, #34), is reaction #35, describing degradation of organic content in order to form CS compounds, with the value of normalized sensitivity coefficient of 0.248 (Fig. 7). That means if the rate of the formation of CS compounds throughout reaction #35 increases, the concentration of IP would decrease. This speaks in favor of earlier mentioned assumption that the formation of iron complexes is limiting factor in mineralization yield by dark-Fenton process. Other important reactions according to sensitivity analysis are #1, describing generation of OH radicals through Fenton catalytic cycle, and #8, describing a scavenging nature of H_2O_2 towards OH radicals (Table 1). These two reactions have values of normalized sensitivity coefficients 1 order of magnitude lower than reaction #35 (Table 1), indicating to their minor influence on the mineralization rate. The index of normalized sensitivity coefficient for reaction #1 is negative indicating that an increase in its rate constant would led to the generation of OH radicals in higher concentration resulting with higher yield of mineralization. On the other hand, the index of calculated normalized sensitivity coefficient of reaction #8 is positive, giving the negative influence to the overall mineralization yield due to the scavenging nature of H_2O_2 towards OH radicals. The values of normalized sensitivity analysis of other reactions presented in Fig. 7(A) are 2 or more orders of magnitude lower than the most important reaction for the model for dark-Fenton process, reaction #35. Still, their role is not negligible within the proposed model. Fig. 7(B) presents results of performed sensitivity analysis for model describing system behavior of photo-Fenton process for degradation of RB49 solution. Besides reaction #35, which was again shown as the most important one, other important reactions according to the performed sensitivity analysis are reactions #36 and #38, both with negative indexes of normalized sensitivity coefficients, indicating that an increase in the value of the rate constants would result in the increased yield of mineralization. Other reactions showed on Fig. 7(B) have values of normalized sensitivity coefficient for 2 orders of magnitude less than above mentioned, indicating their less importance in comparison with most important reactions #35, #36, and #38 (Table 1). It should be pointed out that as the most important reaction with positive index, i.e. affecting negatively the mineralization yield, was again shown the reaction #8 which describes scavenging nature of H_2O_2 towards OH radicals.

4.3. Fenton "like", Fe^{3+}/H_2O_2, and photo-Fenton "like", $UV/Fe^{3+}/H_2O_2$, processes

As in the above processes, degradation kinetic of both dyes by the dark-Fenton "like", Fe^{3+}/H_2O_2, and photo-Fenton "like", $UV/Fe^{3+}/H_2O_2$, processes, at earlier established conditions for each dye ($[Fe^{3+}] = 0.5$ mM, $Fe^{3+}/H_2O_2 = 1:10$, pH 3 in the case of RB49 and $[Fe^{3+}] = 0.5$ mM, $Fe^{3+}/H_2O_2 = 1:40$, pH 3 for RB137) is studied [7]. The models developed for Fenton processes were applied in these processes using Fe^{3+} salt as a source of iron catalyst. In Fig. 8 the results of the comparison of model and experimental data for RB49 dye are

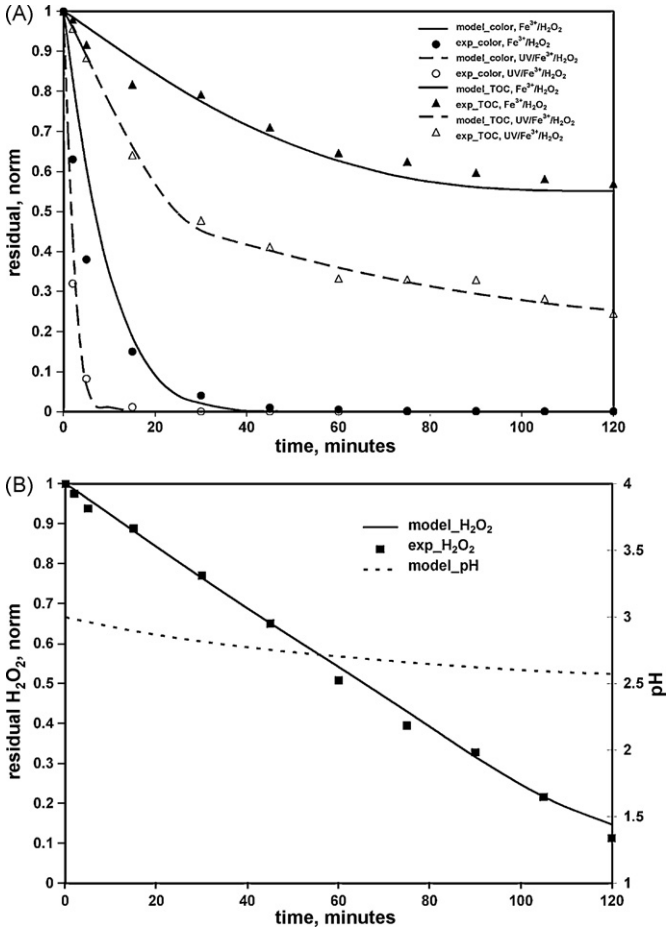

Fig. 8. (A) Degradation kinetic of RB49 by Fe^{3+}/H_2O_2 and $UV/Fe^{3+}/H_2O_2$ processes, the comparison of model and experimental data, (B) H_2O_2 consumption during degradation of RB49 by Fe^{3+}/H_2O_2, the comparison of model and experimental data.

presented. As in the case of dark-Fenton process (Fig. 5), decolorization by dark-Fenton "like" process (Fig. 8) is somewhat slower and at the end reached the value of 98%, while in the case of photo-process the complete decolorization is achieved. If we look only at the decolorization process it can be concluded that it does not matter whether Fe^{2+} or Fe^{3+} salts are used to catalyze the reaction [9]. However, by observing the mineralization process, it is noticeable that not only the rate of mineralization, but also the overall yield of both dark- and photo-processes are lower when Fe^{3+} salts are used. Hence, the final mineralization extents obtained by dark-processes for RB49 are 43.1% by Fe^{3+}/H_2O_2 (Fig. 8) and 74.3% by Fe^{2+}/H_2O_2 (Fig. 5). Observed behavior can be explained by the fact that in the case of processes where Fe^{3+} salt is used as iron catalyst, the generation of OH radicals is limited by much lower reaction rate of the initial reaction. Thereby, in the first step Fe^{3+} ions are reduced to Fe^{2+} ions and HO_2 radicals are formed (Table 1, #2). In the second step Fe^{2+} ions are oxidized to Fe^{3+} and OH radicals are produced (Table 1, #1) [11]. The rate of reaction #2 is 3 orders of magnitude lower than that of reaction #1 ($k_2 = 0.02\ M^{-1}\ s^{-1} \ll k_1 = 76\ M^{-1}\ s^{-1}$), which is the initial reaction in processes using Fe^{2+} salts. Moreover, the reactivity of produced HO_2 radicals (reaction #2) is much lower than that of OH radicals (reaction #1) [9]. Due to the UV assistance, the difference between final mineralization extents for photo-processes using Fe^{3+} and Fe^{2+} salts is somewhat smaller, 77.5% by $UV/Fe^{3+}/H_2O_2$ and 88.5% by $UV/Fe^{2+}/H_2O_2$, in comparison to dark-processes (Figs. 5 and 8). The reason could be found in the synergistic effect of two degradation mechanisms; direct photolysis and OH radicals, which can be generated through several pathways, shown by reaction #1, #26 and #30 (Table 1). However, in photo-Fenton type processes degradation mechanism by OH radicals is predominant over direct photolysis, but depending on the dye structure the participation of organic radicals in chain mechanism should not be neglected, as it was discussed above for RB49. From Fig. 8 and Table 2, a good agreement between experimental and theoretical data for both processes and all observed parameters can be observed. The difference from previous model applied in the case of Fe^{2+} salt is the value of rate constant of reaction #35. The given higher value in the case of Fe^{3+} salt is in accordance with the observed experimental results.

In Fig. 9 the comparison of model and experimental data of degradation kinetics of RB137 by Fe^{3+}/H_2O_2 and $UV/Fe^{3+}/H_2O_2$ processes is shown. It can be seen that as in the case of RB49 (Fig. 8), RB137 is decolorized with lower rate by dark-process than by photo-process, which yielded with somewhat lower final extent. Also, if we compare the results for RB137 presented in Figs. 6 and 9, it can be seen that decolorization rate by dark process using Fe^{3+} salt is lower than by process using Fe^{2+}. As mentioned earlier, in the case of Fe^{3+} salt the generation of OH radicals, as a main oxidative specie responsible for degradation of present organic pollutant, is limited by much lower reaction rate of the initial reaction of Fenton catalytic cycle ($k_2 = 0.02\ M^{-1}\ s^{-1} \ll k_1 = 76\ M^{-1}\ s^{-1}$). On the other hand, decolorization rates of RB137 obtained by both Fe^{3+} and Fe^{2+} photo-processes are almost the same. It can be concluded that the negative effect of slower initial reaction in Fe^{3+}/H_2O_2 system is compensated by UV assistance. The similar trends of both mineralization curves presented in Figs. 6 and 9 can be observed. After the initial period of relatively fast mineralization, process in the dark is almost inhibited in both cases, supporting the above mentioned degradation pathway of RB137 by Fenton type processes towards forming iron-complexing species as a dye degradation products. Due to the previously given explanation, lower mineralization extent could be expected in the process using Fe^{3+} salt. In that case, discrepancy with obtained results can be observed. However, if we look closely at mineralization curves, it can be seen that in the case of Fe^{3+} salt initial mineralization proceeds with lower rate. As a consequence, the formation of iron-complexes is delayed resulting with higher overall mineralization extent. Namely, 45.3% of TOC is removed by Fe^{3+}/H_2O_2 (Fig. 9), while Fe^{2+}/H_2O_2 yielded only 34.3% (Fig. 6). On the other hand, the photo-process using Fe^{3+} salt provided expected results: lower mineralization rate yielding with final lower TOC removal than in the case of process using Fe^{2+} salt. After initial 15 min during which mineralization curves of dark- and photo-processes are almost overlapping, the mineralization by $UV/Fe^{3+}/H_2O_2$ proceeds due to the degradation of formed iron-complexes resulting with 79.4% of TOC removal (Fig. 9). Again, like in the above case of RB49, it can be seen that developed models followed the experimentally obtained results with high accuracy (calculated SD values are shown in Table 2).

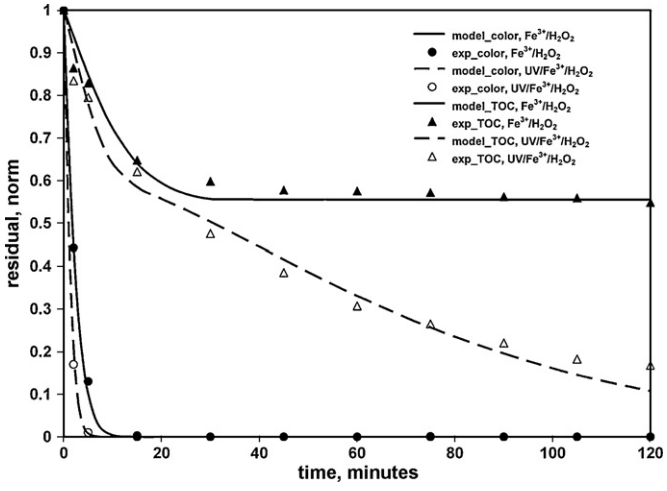

Fig. 9. Degradation kinetic of RB137 by Fe^{3+}/H_2O_2 and $UV/Fe^{3+}/H_2O_2$ processes, the comparison of model and experimental data.

4.4. Fenton "like", Fe^0/H_2O_2, and photo-Fenton "like", $UV/Fe^0/H_2O_2$, processes

The kinetic of third group of applied processes, where iron powder is used as a source of catalysts in Fenton reaction is studied in the same manner as the above presented homogeneous Fenton type processes. For RB49 dye 28 mg L^{-1} of iron powder is added, corresponding to $c(Fe^0) = 0.5$ mM, while the Fenton ratio was $Fe^0/H_2O_2 = 1{:}20$ and pH 3. Fig. 10 summarizes the kinetic of decolorization and mineralization of RB49 by both heterogeneous Fenton type processes, Fe^0/H_2O_2 and $UV/Fe^0/H_2O_2$ (A), as well as consumption of H_2O_2 and leaching of iron ions from solid surface into the bulk (B). On the basis of earlier developed model for homogeneous processes, the models describing heterogeneous processes were developed using the knowledge from the literature related with behavior of iron powder and heterogeneous Fenton catalysts in similar environment [11,25,26,31]. From the modeling point of view, it can be concluded that developed models describe system behavior with a high accuracy; SD ranging for all model–experiment data pairs from 0.0063 to 0.0288 (Table 2). It can be seen that decolorization obtained by dark-process is somewhat slower than that obtained by photo-process, similarly as in the case of two previously presented processes. But heterogeneous dark-process yielded 100% decolorization (Fig. 10), which was not the case in both homogeneous dark-processes (Figs. 5 and 8). By comparing Figs. 5, 8 and 10 it can be observed that initial mineralization rate of RB49 by Fe^0/H_2O_2 process is significantly lower than by Fe^{2+}/H_2O_2 and similar to that by Fe^{3+}/H_2O_2 process. Lower initial mineralization rate in process using iron powder is consequence of slow leaching of iron, providing Fe^{2+} for initiating Fenton cycle in the bulk [25]. On the other hand, in heterogeneous processes, Fen-

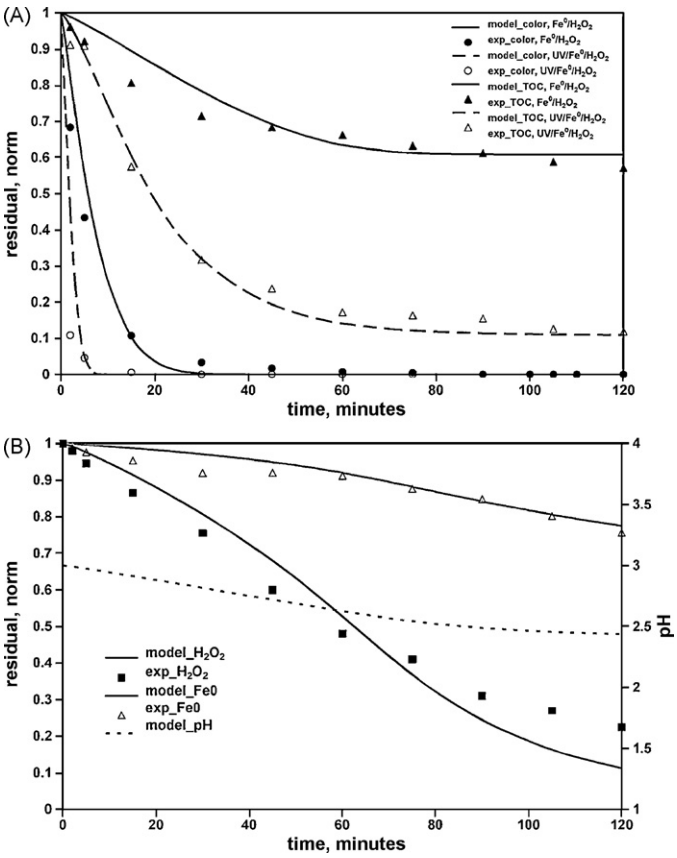

Fig. 10. (A) Degradation kinetic of RB49 by Fe^0/H_2O_2 and $UV/Fe^0/H_2O_2$ processes, the comparison of model and experimental data, (B) H_2O_2 consumption and the leaching of iron ions from iron powder surface during degradation of RB49 by Fe^0/H_2O_2, the comparison of model and experimental data.

ton reactions are also taking place on the surface of solid particles [11], with the induction period characteristic for all heterogeneous catalytic systems. The pronounced leveling off of mineralization kinetic curve by dark-process using iron powder led to the conclusion that iron-complexes are formed in the bulk same as in homogeneous processes (Figs. 5 and 8). It should be pointed out that in Fe^0/H_2O_2 process, the concentration of free iron ions is lower in comparison to the processes using iron salt, even up to three times lower, i.e. the concentration of iron ions in the bulk after the treatment by processes using iron powder and iron salts were 0.17 and 0.5 mM respectively (Fig. 10(B)). Also, those complexes can be formed on the solid surface thus lowering number of free active sites resulting with decreasing the overall concentration of OH radicals in the system [44]. However, due to the leaching of iron from solid phase, mineralization is continued, but with lower rate. As it was expected, the efficiency of Fe^0/H_2O_2 is enhanced by UV assistance yielding with 88.2% of TOC removal which is twice higher than in the dark.

Similar results are obtained for RB137 degradation (Fig. 11). Decolorization is complete after 1 h of treatment in both cases. Moreover, overlapping curves indicate that decolorization proceeds with the same rate. Again, developed models showed good accordance with experimental data (Table 2). However, it should be emphasized that all models in this study are developed on the basis of the results of laboratory batch experiments using model pollutants in low concentration. Real dye wastewater may differ depending on the characteristics of present pollutant and further modification of developed models may be required, which is in accordance with the results of the study indicating that degradation pathways depend on dye structure.

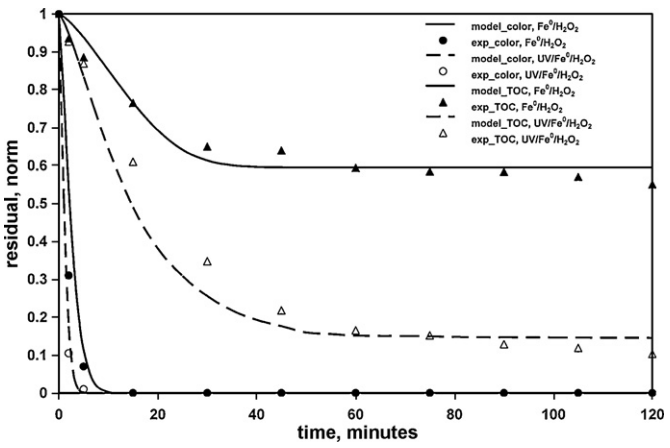

Fig. 11. Degradation kinetic of RB137 by Fe^0/H_2O_2 and $UV/Fe^0/H_2O_2$ processes, the comparison of model and experimental data.

From Figs. 10 and 11 it can be seen that, except for decolorization within 60 min of treatment by process using iron powder in the dark due to the easier cleavage of azo than anthraquinone chromophore [35], there are no other differences related to different dye structure of RB49 and RB137 dyes, as it was shown in homogeneous processes. Moreover, Fe^0/H_2O_2 and $UV/Fe^0/H_2O_2$ processes yielded with the same decolorization and similar mineralization extents for both dyes and processes. If iron powder is considered only as a source of free iron ions in the bulk, the system behavior should be similar to the above shown homogeneous processes. The obtained results lead to the conclusion that this was not the case and that reactions taking place at the solid surface play significant role in overall process effectiveness of heterogeneous processes. This statement is supported by the results of sensitivity analysis performed for model describing the behavior of dark process using iron powder as a source of Fenton catalyst (Fig. 12). Calculated values of the normalized sensitivity coefficients for the reactions occurring at the solid surface are at least 1 order of magnitude higher than for those in the bulk, speaking in favor of the above stated significance of the surface reactions. Reaction #35 describing the formation of CS compounds, was earlier determined as the most important in homogeneous process. Hence, this reaction was shown to be the most important in heterogeneous process too, with normalized sensitivity coefficient of 0.608 (not included in Fig. 12). Other reactions describing the system behavior have 2 or more orders of magnitude lower coefficients (Fig. 12).

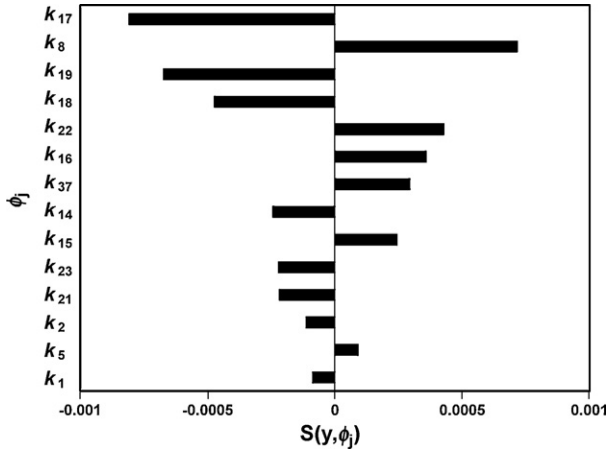

Fig. 12. The peak values of the normalized sensitivity coefficients for the concentration of inorganic products (IP) with respect to reaction rate constant for the chemical reactions used in kinetic modeling; for dark-Fenton type process using iron powder.

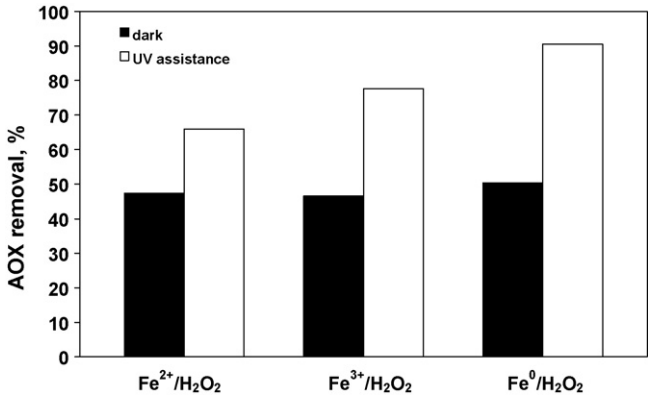

Fig. 13. Comparison of AOX removal by dark- and photo-Fenton type processes in the case of RB49.

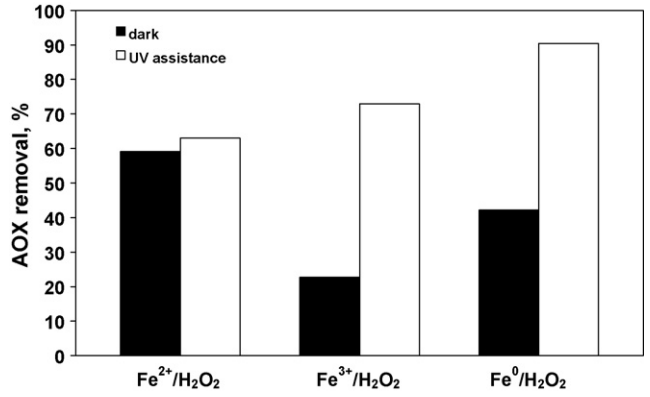

Fig. 14. Comparison of AOX removal by dark- and photo-Fenton type processes in the case of RB137.

At the end, as it was discussed above in Section 4.1, chlorinated triazine structures are less resistant to degradation under UV irradiation than other aromatic or aliphatic intermediates of partial dye degradation. According to Figs. 13 and 14, it is obvious that UV irradiation enhanced process effectiveness in the case of both studied dyes and all applied Fenton type processes in the terms of AOX removal. It can be concluded that degradation of all chlorinated structures is more favorable under UV irradiation. However, from the presented results the direct correlation between TOC and AOX parameters cannot be drawn. Comparing the results of AOX removal by homogeneous processes it can be concluded that halogenated structures amounts differently in overall residual organic content expressed by the means of sum parameter TOC (final extents at Figs. 5–11). This speaks in favor of different degradation pathways depending on dye structure and the type of Fenton reagent.

5. Conclusions

The kinetic of dark- and photo-Fenton and Fenton "like" processes for the treatment of model dye wastewater was studied. Both dark- and photo-Fenton type processes were shown to be very efficient for overall color removal, >98%. It has been shown that decolorization rates are enhanced by assistance of UV irradiation in the case of both studied dyes and all applied Fenton type processes. This effect is even more pronounced in the case of mineralization where significant improvements were achieved, both in final extents and rates. Also, according to the obtained AOX removals, it can be concluded that UV irradiation significantly improved the degradation of either chlorotriazine part of parent dye molecules or formed chlorinated by-products. The improvement in the overall process efficiency by UV irradiation can be mainly contributed to the degradation of Fe^{3+}-complexes restraining Fenton catalytic cycle in the dark. In photo-Fenton type processes additional source of OH radical throughout the photolysis of H_2O_2 is provided contributing to the overall process effectiveness. Depending on dye structure and process type different degradation mechanisms can be assumed manifesting with the different ratio of residual overall organic and halogenated organic content. In the case of Fenton processes using iron powder, Fenton reactions both in the bulk and at the solid surface are taking place. Thus, in comparison to homogeneous Fenton type processes, similar decolorization and mineralization extents can be achieved, while the lower amount of iron ions is present in the bulk after the treatment. Moreover, by the utilization of iron powder, the contamination of treated solution with unnecessary counter-ions is avoided, giving heterogeneous Fenton type processes advantage from the environmental point of view.

Developed mathematical models are interpretable and transparent, and with satisfactory accuracy describe mechanisms of dye degradation taking into account reactions occurring in the bulk (homogeneous and heterogeneous system) and at the solid surface (heterogeneous system) in applied Fenton type process. On the basis of the parametric sensitivity analysis performed, the importance of each chemical reaction included in model development was established, indicating that the formation of complex-suitable compounds, dependent on the chemical structure of pollutant, is the limiting factor influencing the overall mineralization extent. Developed models can be used to predict the behavior of the similar systems with the aim of maximizing wastewater treatment process efficiency.

Acknowledgement

We would like to acknowledge the financial support of the Ministry of Education, Science, and Sport, Republic of Croatia (Project No. 125-1253092-1981).

References

[1] A. Riefe, H.S. Freeman, Environmental Chemistry of Dyes and Pigments, John Wiley and Sons, New York, USA, 1996.
[2] D. Phillips, Environmentally friendly, productive and reliable: priorities for cotton dyes and processes, J. Soc. Dyers Colour 112 (1996) 183–186.
[3] R. Nillson, R. Nordlinder, U. Wass, Asthma, rhinitis, and dermatitis in workers exposed to reactive dyes, Br. J. Ind. Med. 50 (1993) 65–70.
[4] A.P. Sincero, G.A. Sincero, Physical-Chemical Treatment of Water and Wastewater, CRC Press, IWA Publishing, New York, USA, 2003.
[5] R.J. Droste, Theory and Practice of Water and Wastewater Treatment, John Wiley and Sons, New York, USA, 1997.
[6] E. Forgacs, T. Cserhati, G. Oros, Removal of synthetic dyes from wastewaters: a review, Environ. Int. 30 (2004) 953–971.
[7] H. Kusic, A. Loncaric Bozic, N. Koprivanac, Fenton type processes for minimization of organic content in coloured wastewaters. Part I: processes optimization, Dyes Pigments 74 (2007) 380–387.
[8] R.J. Bigda, Consider Fenton's chemistry for wastewater treatment, Chem. Eng. Prog. 91 (1995) 62–66.
[9] M.A. Tarr, Fenton and modified Fenton methods for pollutant degradation, in: M.A. Tarr (Ed.), Chemical Degradation Methods for Wastes and Pollutants—Environmental and Industrial Applications, Marcel Dekker, Inc., New York, USA, 2003, pp. 165–200.
[10] V. Kavitha, K. Palanivelu, The role of ferrous ion in Fenton and photo-Fenton processes for the degradation of phenol, Chemosphere 55 (2004) 1235–1243.
[11] H. Kusic, N. Koprivanac, A. Loncaric Bozic, I. Selanec, Photo-assisted Fenton type processes for the degradation of phenol: a kinetic study, J. Hazard. Mater. B136 (2006) 632–644.
[12] F.J. Beltran, Ozone-UV radiation-hydrogen peroxide oxidation technologies, in: M.A. Tarr (Ed.), Chemical Degradation Methods for Wastes and Pollutants—Environmental and Industrial Applications, Marcel Dekker, Inc., New York, USA, 2003, pp. 1–77.
[13] B. Neppolian, H.C. Choi, S. Sakthivel, B. Arabindoo, V. Murugesan, Solar/UV-induced photocatalytic degradation of three commercial textile dyes, J. Hazard. Mater. B89 (2002) 303–317.
[14] I. Peternel, N. Koprivanac, H. Kusic, UV-based processes for reactive azo dye mineralization, Water Res. 40 (2006) 525–532.

[15] H. Kusic, A. Loncaric Bozic, N. Koprivanac, S. Papic, Fenton type processes for minimization of organic content in coloured wastewaters. Part II: combination with zeolites, Dyes Pigments 74 (2007) 388–395.
[16] H. Kusic, N. Koprivanac, L. Srsan, Azo dye degradation using Fenton type processes assisted by UV irradiation: a kinetic study, J. Photochem. Photobiol., A 181 (2006) 195–202.
[17] H. Kusic, N. Koprivanac, A. Loncaric Bozic, S. Papic, I. Peternel, D. Vujevic, Reactive dye degradation by AOPs; development of a kinetic model for UV/H_2O_2 process, Chem. Biochem. Eng. Q. 20 (2006) 293–300.
[18] I. Nicole, J. De Laat, M. Dore, J.P. Duguet, C. Bonnnel, Utilisation du rayonnement ultraviolet dans le traitement des eaux: mesure du flux photonique par actinometrie chimique au peroxyde d'hydrogene [Use of U.V. radiation in water treatment: measurement of photonic flux by hydrogen peroxide actinometry], Water Res. 24 (2) (1990) 157–168.
[19] L.S. Clesceri, A.E. Greenberg, A.D. Eaton, Standard Methods for the Examination of Water and Wastewater Treatment, 20th ed., APHA & AWWA & WEF, USA, 1998.
[20] R. Chen, J.J. Pignatello, Role of quinone intermediates as electron shuttles in Fenton and photoassisted Fenton oxidations of aromatic compounds, Environ. Sci. Technol. 31 (1997) 2399–2406.
[21] N. Kang, D.S. Lee, J. Yoon, Kinetic modeling of Fenton oxidation of phenol and monochlorophenols, Chemosphere 47 (2002) 915–924.
[22] A.A. Burbano, D.D. Dionysiou, M.T. Suidan, T.L. Richardson, Oxidation kinetics and effect of pH on the degradation of MTBE with Fenton reagent, Water Res. 39 (2005) 107–118.
[23] H. Gallard, J. De Laat, Kinetic modelling of Fe(III)/H_2O_2 oxidation reactions in dilute aqueous solution using atrazine as a model organic compound, Water Res. 34 (12) (2000) 3107–3116.
[24] D.R. Grymonpre, W.C. Finney, R.J. Clark, B.R. Locke, Suspended activated carbon particles and ozone formation in aqueous phase pulsed corona discharge reactors, Ind. Eng. Chem. Res. 42 (2003) 5117–5134.
[25] J.A. Bergendahl, T.P. Thies, Fenton's oxidation of MTBE with zero-valent iron, Water Res. 38 (2004) 327–334.
[26] P.G. Tratnyek, Permeable reactive barriers of iron and other zero-valent metals, in: M.A. Tarr (Ed.), Chemical Degradation Methods for Wastes and Pollutants—Environmental and Industrial Applications, Marcel Dekker, Inc., New York, USA, 2003, pp. 371–422.
[27] J.C. Crittenden, S. Hu, D.W. Hand, S.A. Green, A kinetic model for H_2O_2/UV process in a completely mixed batch reactor, Water Res. 33 (10) (1999) 2315–2328.
[28] M. Rodríguez, N.B. Abderrazik, S. Contreras, E. Chamarro, J. Gimenez, S. Esplugas, Iron(III) photoxidation of organic compounds in aqueous solutions, Appl. Catal. B: Environ. 37 (2) (2002) 131–137.
[29] A. Loncaric Bozic, Application of AOPs for organic dye removal from industrial wastewaters, Ph.D. Thesis, University of Zagreb, 2004.
[30] N. Nirmalakhandan, Modeling Tools for Environmental Engineers and Scientists, CRC Press, New York, USA, 2002.
[31] M. Neamtu, C. Catrinescu, A. Kettrup, Effect of dealumination of iron(III)-exchanged Y zeolites on oxidation of Reactive Yellow 84 azo dye in the presence of hydrogen peroxide, Appl. Catal. B 51 (2004) 149–157.
[32] D.R. Grymonpre, A.K. Sharma, W.C. Finney, B.R. Locke, The role of Fenton's reaction in aqueous phase pulsed streamer corona reactors, Chem. Eng. J. 82 (1–3) (2001) 189–207.
[33] A. Varma, H. Morbidelli, H. Wu, Parametric Sensitivity in Chemical Systems, Cambridge University Press, Cambridge, 1999.
[34] M.I. Stefan, UV photolysis: background, in: S.A. Parsons (Ed.), Advanced Oxidation Processes for Water and Wastewater Treatment, IWA Publishing, London, 2004, pp. 7–48.
[35] O. Gimeno, M. Carbajo, F.J. Beltran, F.J. Rivas, Phenol and substituted phenols AOPs remediation, J. Hazard. Mater. B119 (2005) 99–108.
[36] P.W. Atkins, Loncar Physical Chemistry, 5th ed., Oxford University Press, Oxford, UK, 1994.
[37] G.M. Collona, T. Caronna, B. Marcandalli, Oxidative degradation of dyes by ultraviolet radiation in the presence of hydrogen peroxide, Dyes Pigments 41 (1999) 211–220.
[38] W. Feng, D. Nansheng, H. Helin, Degradation mechanism of azo dye C.I. reactive red 2 by iron powder reduction and photooxidation in aqueous solutions, Chemosphere 41 (2000) 1233–1238.
[39] M. Stylidi, D.I. Kondarides, X.E. Verykios, Pathways of solar light-induced photocatalytic degradation of azo dyes in aqueous TiO_2 suspensions, Appl. Catal. B 40 (2003) 271–286.
[40] S. Bilgi, C. Demir, Identification of photooxidation degradation products of C.I. Reactive Orange 16 dye by gas chromatography–mass spectrometry, Dyes Pigments 66 (2005) 69–76.
[41] T. Alapi, A. Dombi, Comparative study of the UV and UV/VUV-induced photolysis of phenol in aqueous solution, J. Photochem. Photobiol., A 188 (2007) 409–418.
[42] J.E.B. McCallum, S.A. Madison, S. Alkan, R.L. Depinto, R.U.R. Wahl, Analytical studies on the oxidative degradation of the reactive textile dye Uniblue A, Environ. Sci. Technol. 34 (24) (2000) 5157–5164.
[43] M. Saquib, M. Muneer, Semiconductor mediated photocatalysed degradation of an anthraquinone dye, Remazol Brilliant Blue R under sunlight and artificial light source, Dyes Pigments 53 (2002) 237–249.
[44] H. Lachheb, E. Puzenat, A. Houas, M. Ksibi, E. Elaloui, C. Guillard, J.-M. Herrmann, Photocatalytic degradation of various types of dyes (Alizarin S, Crocein Orange G, Methyl Red, Congo Red, Methylene Blue) in water by UV-irradiated titania, Appl. Catal. B 39 (2002) 75–90.
[45] R. Comparelli, E. Fanizza, M.L. Curri, P.D. Cozzoli, G. Mascolo, R. Passino, A. Agostiano, Photocatalytic degradation of azo dyes by organic-capped anatase TiO_2 nanocrystals immobilized onto substrates, Appl. Catal. B 55 (2005) 81–91.